Proceedings of ASME 2010 3rd Joint US-European Fluids Engineering Summer Meeting and 8th International Conference on Microchannels and Minichannels
FEDSM2010-ICNMM2010
August 2-4, 2010, Montreal, Canada

FEDSM-ICNMM2010-30857

VALIDATED REDUCED ORDER MODELS FOR SIMULATING TRAJECTORIES OF BIO-INSPIRED ARTIFICIAL MICRO-SWIMMERS

Ahmet Fatih Tabak[*,1] **Serhat Yesilyurt**[*,2]
[*]**Sabanci University, Istanbul, Turkey**
[1]**tabak@sabanciuniv.edu**, [2]**syesilyurt@sabanciuniv.edu**

ABSTRACT
Autonomous micro-swimming robots can be utilized to perform specialized procedures such as in *vitro* or in *vivo* medical tasks as well as chemical surveillance or micro manipulation. Maneuverability of the robot is one of the requirements that ensure successful completion of its task. In micro fluidic environments, dynamic trajectories of active micro-swimming robots must be predicted reliably and the response of control inputs must be well-understood. In this work, a reduced-order model, which is based on the resistive force theory, is used to predict the transient, coupled rigid body dynamics and hydrodynamic behavior of bio-inspired artificial micro-swimmers. Conceptual design of the micro-swimmer is biologically inspired: it is composed of a body that carries a payload, control and actuation mechanisms, and a long flagellum either such as an inextensible whip like tail-actuator that deforms and propagates sinusoidal planar waves similar to spermatozoa, or of a rotating rigid helix similar to many bacteria, such as *E. Coli*. In the reduced-order model of the micro-swimmer, fluid's resistance to the motion of the body and the tail are computed from resistive force theory, which breaks up the resistance coefficients to local normal and tangential components. Using rotational transformations between a fixed world frame, body frame and the local Frenet-Serret coordinates on the helical tail we obtain the full 6 degrees-of-freedom relationship between the resistive forces and torques and the linear and rotational motions of the swimmer. In the model, only the tail's frequency (angular velocity for helical tail) is used as a control input in the dynamic equations of the micro-swimming robot. The reduced-order model is validated by means of direct observations of natural micro swimmers presented earlier in the literature and against; results show very good agreement. Three-dimensional, transient CFD simulations of a single degree of freedom swimmer is used to predict resistive force coefficients of a micro-swimmer with a spherical body and flexible tail actuator that uses traveling plane wave deformations for propulsion. Modified coefficients show a very good agreement between the predicted and actual time-dependent swimming speeds, as well as forces and torques along all axes.

INTRODUCTION
Propulsion mechanisms of biological microorganisms may offer a practical solution to the propulsion of autonomous micro swimming robots [1] which can be used for medical and micro-manipulation tasks. Detailed discussion on propulsion methods and structures of natural micro swimmers, i.e. with both helical and planar wave propagating tails can be found elsewhere [2].

A simple mathematical model of the swimming of spermatozoa with travelling-plane-wave (TPW) deformations is obtained by Gray and Hancock [3]; in the model, one-dimensional forward velocity of the swimmer can be determined from the resistive force theory (RFT). The principle assumption in the RFT is that the local hydrodynamic force on the micro-swimmer is proportional to the local velocity. As pointed out by Sir Lighthill [4], RFT ignores the long range interactions between the body and the flagellum, and between the parts of the flagellum; inclusion of the long-range interactions results in the slender body theory (SBT). Johnson and Brokaw presents an analysis and comparison between the RFT and SBT [5]: in effect, SBT modifies the resistive force coefficients, obtained purely from the geometry of the object with the consideration of long-range interac-

tions, which can only be accounted for only partially as demonstrated by Chattopadhay and Wu [6].

Three-dimensional trajectories of micro swimmers are modeled by Keller and Rubinow [7] using the original RFT, where *X* and *Y*-velocities and *Z*-rotation (3-dof in total) of micro swimming organisms are considered for TPW actuation, and complete 6-dof-swimming is considered for micro-organisms with rigid helical tails using Euler angles and small angle assumption for rotations perpendicular to the direction of the helical rotation. Lauga *et al.* modified the model presented by Keller and Rubinow to include interactions between the swimmer and nearby solid boundaries during the motion of the swimmer [8].

An elasto-hydrodynamic model of the force balance between the internal stress distribution of the solid tail and the resistive force of the fluid is reported in [9]. Takano and Goto introduced a similar resistance coefficient matrix along with internal structural stresses to get fluid forces and studied the effect of helical wave deformation on swimming behavior combined with the forces due to structural deformation of the tail [10].

More powerful numerical tools solving governing differential equations are also employed. Fauci built a finite element framework to conduct numerical experiments on single and multiple planar wave propagating swimmers equipped with different tail morphologies moving inside a confined liquid medium governed by full Navier-Stokes equations [11]. Ramia *et al.* used boundary element method to extract the force coefficients of the drag matrix rather than going through the analytical procedure [12]. Goto *et al.* employed boundary element analysis on velocity, force and torques exerted on a swimmer in micro realm and compared results with statistical data extracted from observations [13].

In this work a mathematical model to obtain the trajectory of a micro swimmer robot is presented. All fluid forces are computed by drag coefficients as resistive force theory suggests. Pure propulsion force and torques from tail deformation are computed regardless of the rigid body motion. Rigid body rotations are handled by Frenet–Serret frames and quaternion computations. Three-dimensional trajectories of micro swimmers are obtained in the lab frame as well as swimmers' own frame. Model is based on an inertia free approach for both fluid dynamics and rigid body dynamics, and proved to be useful on observing the trajectories of the micro swimming robots and organisms.

METHODOLOGY

Swimmer is modeled as fully submerged in a fluidic environment at rest, i.e. with no upstream velocities. Motion of the slender tail is limited to the *q* and *r*-axes by inextensibility assumption as shown in Fig. 1. Both *q*-axis motion and *r*-axis motion of the tail are given by sinusoidal wave-form as a function of time, *t*, position on the tail, *s*, excitation frequency, $2\pi f$, wave number, $k=2\pi L/\lambda$ where *L* is apparent tail length and λ is the wave pitch. Amplitudes B_q and B_r depend on the position, *s*:

$$\begin{aligned} q(s,t) &= B_q(s)\cos(\omega t - ks) \\ r(s,t) &= B_r(s)\sin(\omega t - ks) \end{aligned} \qquad (1)$$

In Eq. (1), B_q and B_r employ a limiting function to define the extent of the deformations as a function of tail position:

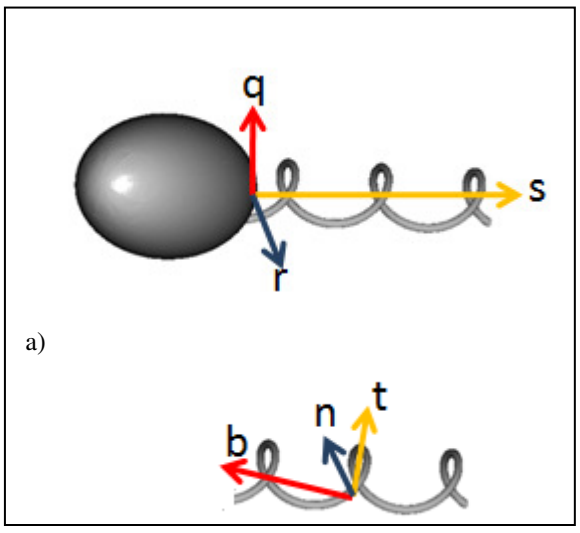

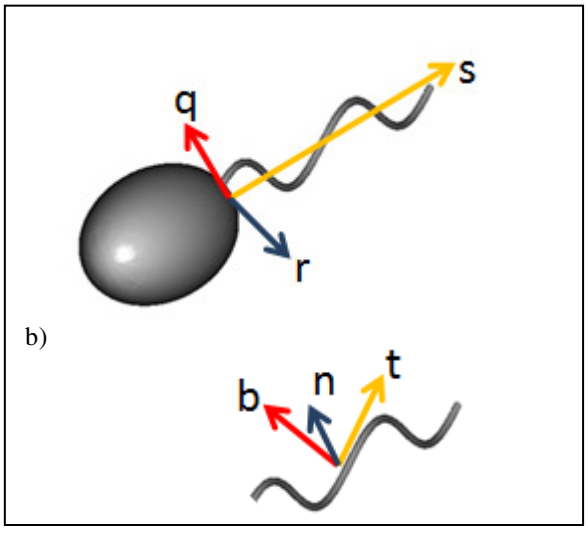

Figure 1: a) Demonstration for an arbitrary swimmer body with helical wave and their respective coordinate frames; b) Demonstration for an arbitrary swimmer body with planar wave and their respective coordinate frames.

$$B_q(s) = B_q^{\max}(1-e^{-cs})$$
$$B_r(s) = B_r^{\max}(1-e^{-cs}) \quad (2)$$

where, c, is the envelope constant. Position of a point on tail is denoted by a position vector $\mathbf{p} = [s\ q\ r]'$ in the body frame. Velocity on tail surface is obtained from the kinematic condition as follows:

$$\mathbf{v}(s) = \frac{d\mathbf{p}}{dt} = \begin{bmatrix} ds/dt \\ dq/dt \\ dr/dt \end{bmatrix} = \begin{bmatrix} 0 \\ -B_q(s)\omega\sin(\omega t - ks) \\ B_r(s)\omega\cos(\omega t - ks) \end{bmatrix} \quad (3)$$

Forces and torques on tail surface are calculated by a 6-by-6 mobility matrix, **C**, and it is derived mainly by imposing rotations on drag coefficients in the *sqr*-frame. Rotation matrix is derived from the local Frenet–Serret coordinates at the tail's surface [14]:

$$\mathbf{t}(s) = \frac{\partial\mathbf{p}/\partial s}{\left\|\partial\mathbf{p}/\partial s\right\|}$$
$$\mathbf{b}(s) = \frac{(\partial\mathbf{p}/\partial s)\times(\partial^2\mathbf{p}/\partial s^2)}{\left\|(\partial\mathbf{p}/\partial s)\times(\partial^2\mathbf{p}/\partial s^2)\right\|} \quad (4)$$
$$\mathbf{n}(s) = \mathbf{b}(s)\times\mathbf{t}(s)$$

The rotation matrix from the local Frenet-Serret coordinates to *sqr*-coordinates of the body is given by:

$$\mathbf{R}_{bnt}^{sqr} = \left[\mathbf{b}(s) \quad \mathbf{n}(s) \quad \mathbf{t}(s)\right] \quad (5)$$

The force and torque vector can be written as a linear function of velocities in *sqr*-frame and drag matrix as follows:

$$\begin{bmatrix} \mathbf{F}_{tail}^{sqr} \\ \mathbf{T}_{tail}^{sqr} \end{bmatrix} = \begin{bmatrix} \mathbf{C}_U^F & \mathbf{C}_\omega^F \\ \mathbf{C}_U^T & \mathbf{C}_\omega^T \end{bmatrix} \begin{bmatrix} \mathbf{U}_{tail}^{sqr} \\ \boldsymbol{\omega}_{tail}^{sqr} \end{bmatrix} \quad (6)$$

where each **C** is a 3-by-3 matrix, superscript F denotes the contribution to force vector, superscript T denotes the contribution to torque vector. Similarly, subscript U denotes the contribution from linear velocities and subscript ω denotes the contribution from angular velocities. Components of the tail's mobility matrix are obtained as follows:

$$\mathbf{C}_U^F = \int \mathbf{C}_{RR} ds \quad (7)$$

$$\mathbf{C}_U^T = \int \mathbf{p}\times\mathbf{C}_{RR} ds \quad (8)$$

$$\mathbf{C}_\omega^F = \int \mathbf{C}_{RR}\mathbf{S} ds \quad (9)$$

$$\mathbf{C}_\omega^T = \int \mathbf{p}\times(\mathbf{C}_{RR}\mathbf{S}) ds \quad (10)$$

In (7)-(10), $\mathbf{C}_{RR}$ is the point-wise contribution of the local resistive force coefficients on the body frame and **S** is the local skew-symmetric matrix based on position vector components; $\mathbf{C}_{RR}$ and **S** are given as follows:

$$\mathbf{C}_{RR} = \mathbf{R}_{bnt}^{sqr}\begin{bmatrix} -C_n & 0 & 0 \\ 0 & -C_n & 0 \\ 0 & 0 & -C_t \end{bmatrix}\left(\mathbf{R}_{bnt}^{sqr}\right)^t \quad (11)$$

$$\boldsymbol{\omega}\times\mathbf{p} = \mathbf{S}\boldsymbol{\omega} = -\begin{bmatrix} 0 & -r(s,t) & q(s,t) \\ r(s,t) & 0 & -s \\ -q(s,t) & s & 0 \end{bmatrix}\boldsymbol{\omega} \quad (12)$$

In (11), C_n and C_t are normal and tangential force coefficients of tail.

Assuming that the center of mass of the swimmer close enough to the body center of mass, the force (and torque)-velocity (and angular velocity) relationship for the body is given by:

$$\begin{bmatrix} \mathbf{F}_{body}^{sqr} \\ \mathbf{T}_{body}^{sqr} \end{bmatrix} = \begin{bmatrix} \mathbf{D}_U^F & 0 \\ 0 & \mathbf{D}_\omega^T \end{bmatrix}\begin{bmatrix} \mathbf{U}_{body}^{sqr} \\ \boldsymbol{\omega}_{body}^{sqr} \end{bmatrix} \quad (13)$$

In (13), **D** is a 3-by3 matrix and the contributions from linear and angular velocities are obtained from that of a spherical body:

$$\mathbf{D}_U^F = \begin{bmatrix} -6\pi\mu r^2 & 0 & 0 \\ 0 & -6\pi\mu r^2 & 0 \\ 0 & 0 & -6\pi\mu r^2 \end{bmatrix} \quad (14)$$

$$\mathbf{D}_\omega^T = \begin{bmatrix} -8\pi\mu r^3 & 0 & 0 \\ 0 & -8\pi\mu r^3 & 0 \\ 0 & 0 & -8\pi\mu r^3 \end{bmatrix} \quad (15)$$

where, μ is dynamic viscosity of the surrounding fluid and, r is the spherical body radius. In case of non-spherical objects Eq. (14)-(15) differ [15] and can be determined numerically

The velocity vectors are written as follows:

$$\mathbf{U}_{body}^{sqr} = \left[u_{sw}^s \quad u_{sw}^q \quad u_{sw}^r\right]'$$
$$\mathbf{U}_{tail}^{sqr} = \left[u_{sw}^s \quad u_{sw}^q \quad u_{sw}^r\right]' + d\mathbf{p}/dt \quad (16)$$

$$\boldsymbol{\omega}_{tail}^{sqr} = \left[\omega_{tail}^s \quad \omega_{sw}^q \quad \omega_{sw}^r\right]'$$
$$\boldsymbol{\omega}_{body}^{sqr} = \left[\omega_{body}^s \quad \omega_{sw}^q \quad \omega_{sw}^r\right]' \quad (17)$$

and subscript *sw* denotes the swimmer.

For an untethered swimmer, the sum of force and torque vectors should give zero net force and torque

for the micro swimmer in the reference world frame. This leads up to the 6-dof equation of motion of the micro-swimmer:

$$\mathbf{F}_{tail} + \mathbf{F}_{body} = 0 \tag{18}$$

Up-to-date orientation with respect to the original position in *sqr*-frame due to complex rotations is handled by quaternion [16] integration as follows:

$$\begin{aligned} \mathbf{q}_{sqr}^{XYZ} &= \begin{bmatrix} q_{s0} & q_{v1} & q_{v2} & q_{v3} \end{bmatrix} \\ \mathbf{R}_{sqr}^{XYZ} &= \begin{bmatrix} R_{11} & R_{12} & R_{13} \\ R_{21} & R_{22} & R_{23} \\ R_{31} & R_{32} & R_{33} \end{bmatrix} \end{aligned} \tag{19}$$

where $\mathbf{q}$ is the quaternion structure with one scalar value denoted by the subscript $s0$ and three vector components denoted by subscripts $v1$, $v2$ and $v3$. Corresponding instantaneous rotation matrix can be derived as follows:

$$\begin{aligned} R_{11} &= 1-2\left(q_{v2}\right)^2-2\left(q_{v3}\right)^2 \\ R_{12} &= 2q_{v1}q_{v2}-2q_{v3}q_{s0} \\ R_{13} &= 2q_{v1}q_{v3}+2q_{v2}q_{s0} \\ R_{21} &= 2q_{v1}q_{v2}+2q_{v3}q_{s0} \\ R_{22} &= 1-2\left(q_{v1}\right)^2-2\left(q_{v3}\right)^2 \\ R_{23} &= 2q_{v2}q_{v3}-2q_{v1}q_{s0} \\ R_{31} &= 2q_{v1}q_{v3}-2q_{v2}q_{s0} \\ R_{32} &= 2q_{v2}q_{v3}+2q_{v1}q_{s0} \\ R_{33} &= 1-2\left(q_{v1}\right)^2-2\left(q_{v2}\right)^2 \end{aligned} \tag{20}$$

The time derivative of quaternion is computed as

$$\dot{\mathbf{q}}_{sqr}^{XYZ} = \begin{bmatrix} \dot{q}_{s0} & \dot{q}_{v1} & \dot{q}_{v2} & \dot{q}_{v3} \end{bmatrix} \tag{21}$$

with an individual formulation for both parts:

$$\begin{aligned} \dot{q}_{s0} &= -\left(\omega_{sw}^{s}q_{v1}+\omega_{sw}^{q}q_{v2}+\omega_{sw}^{r}q_{v3}\right)/2 \\ \begin{bmatrix} \dot{q}_{v1} \\ \dot{q}_{v2} \\ \dot{q}_{v3} \end{bmatrix} &= q_{s0}\begin{bmatrix} \omega_{sw}^{s} \\ \omega_{sw}^{q} \\ \omega_{sw}^{r} \end{bmatrix} + \begin{bmatrix} \omega_{sw}^{s} \\ \omega_{sw}^{q} \\ \omega_{sw}^{r} \end{bmatrix} \times \begin{bmatrix} q_{v1} \\ q_{v2} \\ q_{v3} \end{bmatrix} \end{aligned} \tag{22}$$

which will be integrated over time to obtain current quaternion at each time for extend of simulation.

RESULTS

The validity of the model is verified with CFD simulations for a spherical body with a tail carrying out planar wave propagation. CFD simulations are governed by full Navier-Stokes Equations on a moving deforming mesh according to the Arbitrary Lagrangian Eulerian formulation that follows the motion of the swimmer [17]. Commercial software package COMSOL is used in simulations [18]. Each CFD simulation requires about 35K total number of degrees of freedom, and takes at least 10 minutes on a 16 GB Xeon system working on Linux. Reduced-order-model simulations based on RFT take less than two seconds using 50 segments per wavelength on the tail. Parameters used in the simulations are listed in Table 1 and results are depicted in Fig. (2)-(5).

Name of Property	Value
Fluid density, ρ	1 [1]
Dynamic Viscosity, μ	1.12 [1]
Driving Frequency, f	1 [Hz]
Tail length, L	0.35 [1]
Wave Length, λ	0.175 [1]
Envelope constant, c	6 [1]
Wave amplitude, B	$5\text{x}10^{-3}$ [1]
Body radius, r	$5\text{x}10^{-2}$ [1]
Tail radius, d	$1\text{x}10^{-3}$ [1]
Length Scale, l	$1\text{x}10^{-3}$ [m]
Channel width, w	1.6 [1]
Channel height, h	1.6 [1]

Table 1: Geometry and material information for CFD based 1-dof time dependent behavior presented in Figs. (2)-(5).

Two sets of RFT coefficients are employed: one set is based on asymptotic approximations reported in the literature, and the other is obtained from CFD simulations. Sir Lighthill obtained following coefficients based on an asymptotic solution of the flow around a flagellum with traveling-plane wave deformations [4]:

$$\begin{aligned} C_t &= 4\pi\mu \Big/ \left(-1+\log\left(\left(\lambda e^{-0.577/\pi/d}\right)^2\right)\right) \\ C_n &= 8\pi\mu \Big/ \left(1+\log\left(\left(\lambda e^{-0.577/\pi/d}\right)^2\right)\right) \end{aligned} \tag{22}$$

Alternatively, Johnson and Brokaw obtained following coefficients under the based on the slender body theory, in which interactions between the body and the tail are considered [5]:

$$\begin{aligned} C_t &= 4\pi\mu \Big/ \left(1/2+\log\left(\left(2\lambda/d\right)^2\right)\right) \Big/ 1.7 \\ C_n &= 4\pi\mu \Big/ \left(1/2+\log\left(\left(2\lambda/d\right)^2\right)\right) \end{aligned} \tag{23}$$

In (22) and (23), d is the radius of the tail.

In Fig. 2, comparisons of the time-dependent X-velocity of the swimmer are shown. In the CFD code, total fluid forces and torques acting on the swimmer are calculated by integrating the total stress tensor components in all directions. The velocity of the

swimmer moving in the *X*-direction is calculated by the constraint equation that the total force on the swimmer in the *X*-direction must be zero by using global equations (constraints) in COMSOL [18]. Working backwards from the results, the RFT coefficients that satisfy the balance in that direction are calculated from the CFD simulation results, and used in the RFT-based reduced-order model. Comparisons of the reduced-order model results with the Lighthill's coefficients, coefficients obtained from the CFD simulation and the CFD simulation are shown in Fig. 2. According to the results, RFT coefficients obtained from the CFD simulations compare very well with the CFD simulation results.

Furthermore, for an anchored swimmer, total forces along *X* and *Y*-directions and the torque along the *Z*-direction calculated from CFD simulations are compared with the forces obtained from the reduced-order model simulations, which, in effect, are the propulsion force components since RFT does not account for flow interactions between the tail and the body. In Fig. 3, *X*-direction force, which is calculated from the simple model with coefficients obtained from the CFD simulations of the moving swimmer, agrees very well with the forces obtained from the CFD simulations of the stationary swimmer; in comparison forces obtained from the simple model using resistive-force coefficients given in (22).

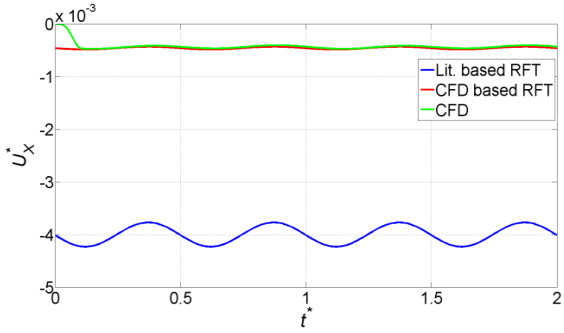

Figure 2: Time dependent dimensionless forward velocities for micro swimmer; CFD vs. RFT.

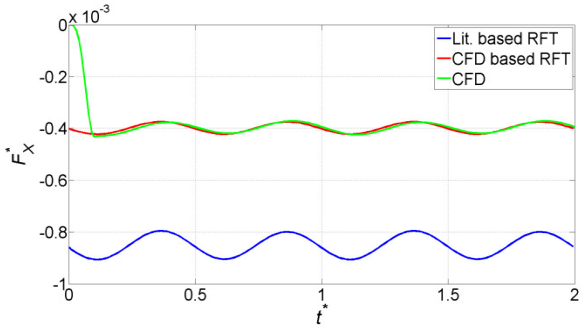

Figure 3: Time dependent dimensionless *X*-force for anchored swimmer; CFD vs. RFT.

In Fig. 4 and Fig. 5, forces along the *Y*-direction and torque along the *Z*-direction are shown. Resistive-force coefficients obtained from CFD simulations perform considerably better than the ones given in (22) in both cases.

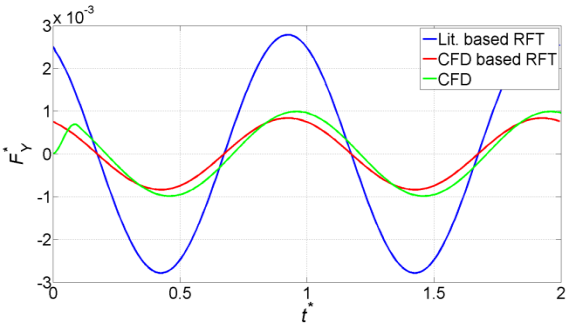

Figure 4: Time dependent dimensionless *Y*-force for anchored swimmer; CFD vs. RFT.

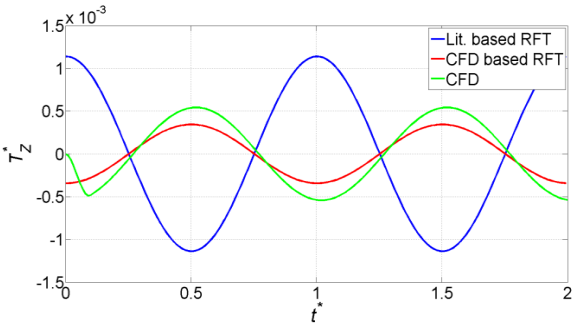

Figure 5: Time dependent dimensionless *Z*-torque for anchored swimmer; CFD vs. RFT

Moreover, since CFD simulations require boundary conditions away from swimmer body, there exists an interaction between the flow field created by the wave propagation along the deforming tail and channel boundaries. This interaction of flow field may contribute to the small deviation in time dependent forces, torque and the velocity as shown in Figs. (2)-(5). In effect, anchored tail creates a flow in the channel, which introduces additional *XY*-forces and the *Z*-torque on the swimmer somewhat different than the ones acting on the stationary swimmer placed in a fluid at rest.

The brief transient behavior detected in CFD simulations is due to the developing effect of the steady periodic flow surrounding the micro swimmer due to tail deformation as shown in Fig. 6.

Due to the lack of information on 6-dof motion behavior in literature, only time averaged forward velocities are compared in the lab frame, i.e. *XYZ*-frame, for particular swimmers presented by Brennen and Winet [2] and Chattopadhyay [6].

Furthermore, observations for natural swimmers presented in literature are used for the validation of the RFT model for the helical swimmer. Three species listed in Table 2 are reported to employ helical wave propagation and a revolute joint resides in between their body and tail [6]. In comparison, four

species listed in Table 3 are reported containing bio-physical actuators resulting in plane wave deformations [2].

RFT results obtained from coefficients suggested by Johnson and Brokaw [5] are found to be more agreeable with the reported forward velocities [2], [6]. Only exemption is the *V.Alginolyticus* [6] which is found to agree better with the coefficients suggested by Sir Lighthill [4].

Name of the Species	Observed Forward Velocity [m/s]	Computed Forward Velocity [m/s]
V.Alginolyticus	$34x10^{-6}$	$39x10^{-6}$ [4]
C.Crescentus	$30x10^{-6}$	$34x10^{-6}$ [5]
E.Coli	$14x10^{-6}$	$11x10^{-6}$ [5]

Table 2: Validation results for observation data on bacteria employing helical wave propagation as propulsion method in literature [6].

Name of the Species	Reported (Literature) Forward Velocity	Computed (RFT) Forward Velocity
Tenebrio Spermatozoa	$67x10^{-5}$ [m/s]	$54x10^{-5}$ [m/s]
Lytechinus Spermatozoa	$99x10^{-5}$ [m/s]	$60x10^{-5}$ [m/s]
Ciona Spermatozoa	$10x10^{-6}$ [m/s]	$72x10^{-5}$ [m/s]
Chaetopterus Spermatozoa	$65x10^{-5}$ [m/s]	$50x10^{-5}$ [m/s]

Table 3: Validation results for observation data on spermatozoa employing planar wave propagation as propulsion method in literature [2].

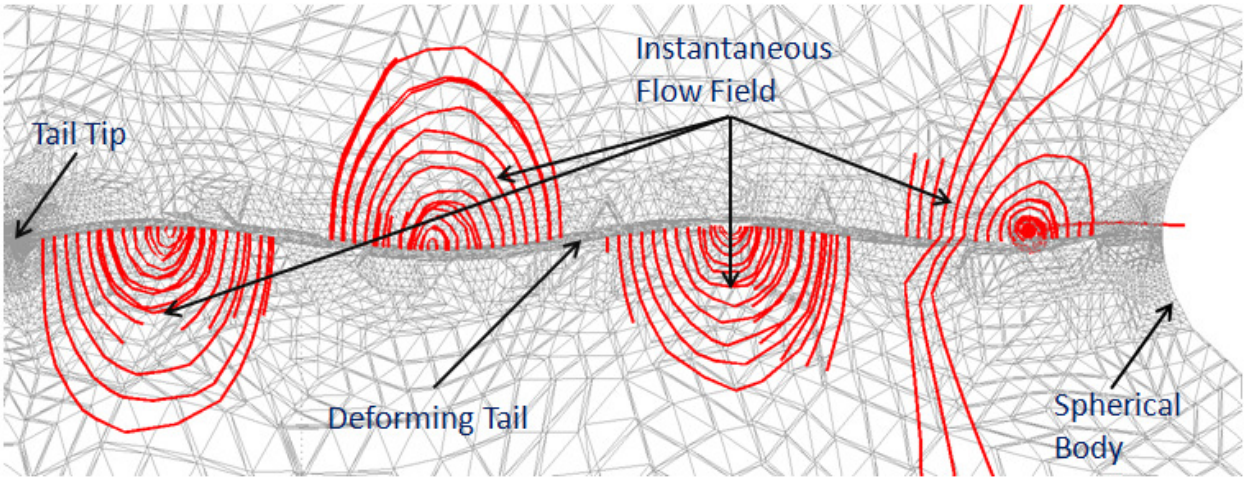

Figure 6: Close up view on the overall meshing and the instantaneous flow field around the deforming tail; computed in CFD simulations.

CONCLUSION

The reduced-order model based on RFT, which is used to model the motion of micro swimming robots, predicts swimming speed of natural swimmers and forces produced by the motion of the tail, which are calculated by CFD simulations. The model can be used to obtain trajectories of micro swimmers that use rotation of rigid helical tails or TPW propagation of deformation on their tails for propulsion. Based on the RFT coefficients suggested in literature, model compares well, within 30%, with the observed average swimming velocities of natural micro swimmers.

Moreover, RFT coefficients obtained from simple CFD simulations can be used to obtain accurate results for arbitrary viscous swimmers. The swimming trajectories obtained from the reduced-order model can be used in design optimization studies, and navigation and control of micro swimming robots which can be utilized in micro manipulation and medical tasks.

REFERENCES

[1] Edd, J., Payen, S., Rubinsky, B., Stoller, M.L., Sitti, M., 2003, "Biomimetic Propulsion for a Swimming Surgical Micro-Robot," IEEE/RSJ Intelligent Robotics and Systems Conference, Las Vegas, USA.

[2] Brennen, C., Winet, H., "Fluid Mechanics of Propulsion by Cilia and Flagella", Ann. Rev. Fluid Mech., Vol. 9, pp. 339-398, 1977.

[3] Gray, J., Hancock, G.J., "The Propulsion of Sea-Urchin Spermatozoa", J. Exp. Biol., Vol.32, pp. 802-814, 1955.

[4] Lighthill, Sir J., "Mathematical Biofluiddynamics", Society for Industrial and Applied Mathematics, USA, Ch. 3, 1975

[5] Johnson, R.E., Brokaw, C.J., "Flagellar Hydrodynamics A Comparison between Resistive-Force Theory and Slender Body Theory", Biophys. J., Vol. 25, pp. 113-127, 1979.

[6] Chattopadhyay, S., Wu, X.-L., "The effect of Long-Range Hydrodynamic Interaction on the Swimming of a Single Bacterium", Biophysical Journal, Vol. 96, pp. 2023-2028, 2009.

[7] Keller, J.B., Rubinow, S.I., "Swimming of Flagellated Microorganisms", Biophysical Journal, Vol. 16, pp. 151-170, 1976.

[8] Lauga, E., DiLuzio, W.R., Whitesides, G.M., Stone, H.A., "Swimming in Circles: Motion of Bacteria near Solid Boundaries", Biophysical Journal, Vol. 90, pp. 400-412, 2006.

[9] Spagnolie, S.E., Lauga, E., "The Optimal Elastic Flagellum", Physics of Fluids, Vol. 22, 031901, 2010.

[10] Takano,Y., Goto, T., "Numerical Analysis of Small Deformation of Flexible Helical Flagellum of Swimming Bacteria", JSME International Journal, Series C, Vol. 46, No. 4, pp. 1234-1240, 2003.

[11] Fauci, L.J., A Computational Model of the Fluid Dynamics of Undulatory and Flagellar Swimming", Amer. Zool., Vol. 36, pp. 599-607, 1996.

[12] Ramia, M., Tullock, D.L., Phan-Thien, N., "The Role of Hydrodynamic Interaction in the Locomotion of Microorganisms", Biophysical Journal, Vol. 65, pp. 755-778, 1993.

[9] De la Torre, J.G., Bloomfield, V.A., "Hydrodynamic Theory of Swimming of Flagellated Microorganisms", Biophysical Journal, Vol. 20, pp. 49-67, 1977.

[10] Gauger, E., Stark, H., "Numerical Study of a Microscopic Artificial Swimmer", Physical Review, Ser. E, Vol. 74, 021907, 2006.

[11] Keaveny, E.E., Maxey, M.R., "Spiral Swimming of an Artificial Micro-Swimmer", J. Fluid Mech., Vol. 598, pp. 293-319, 2008.

[12] Brokaw, C.J., "Non-Sinusoidal Bending Waves of Sperm Flagella", J. Exp. Biol., Vol. 43, pp. 155-169, 1965.

[13] Goto, T., Masuda, S., Terada, K., Takano, Y., "Comparison between Observation and Boundary Element Analysis of Bacterium Swimming Motion", JSME International Journal, Series C, Vol. 44, No. 4, pp. 958-963, 2001.

[14] Hanson, A.J., Ma, H., "Visualizing Flow with Quaternion Frames", Proceedings of the conference on Visualization '94, Washington, D.C., pp. 108 – 115, 1994.

[15] Perrin, F., "Mouvement Brownien d'un Ellipsoide (II). Rotatıon Libre et Dépolarisation des Fluorescences. Translation et Diffusion de Molécules Ellipsoidale ", Le Journal De Physique, Series VII, Tome. VII, No. 1, pp. 1-11, 1936.

[16] Baraff, D., "Physical Based Modeling, Rigid Body Simulation", Siggraph 2001 Course Notes, pp. G1-G68, 2001.

[17] Duarte, F., Gormaz, R., Natesan, S., "Arbitrary Lagrangian-Eulerian Method for Navier-Stokes Equations with Moving Boundaries", Comput. Methods Appl. Mech. Engrg., 193, pp. 4819-4836, 2004.

[18] COMSOL AB, *Comsol Multiphysics User's Guide*, 2010.